A study of Platinum metal as a component of fuel cells

K.N. Nigussa
Department of Physics, Addis Ababa University, P.O.box 1176, Ethiopia

Abstract— Adsorption energies of small molecules carbon monoxide and hydrogen are studied using density functional theory and the neural network method of generating higher dimensional potential energy surfaces. Various lower index surfaces of platinum metal are considered, and the adsorption energies appear to increase according to: Pt (211) > Pt (100) > Pt (110) > Pt (111) with the adsorption of both molecules. The large adsorption energies mean only energetic interactions with the ions from air such as oxygen ion can detach the adsorbates from the surface thereby forming water and carbon monoxide as by-products. Exploring possible adsorption sites gives insight on better ways in which charge exchanges are maximized while at the same time forming of the by-products becomes efficient. The adsorption energies range between 0.85 eV to 2.08 eV with the adsorption of CO while the values are between 1.30 eV to 1.9 eV with the adsorption of hydrogen. Charge transfers give some insight into the study of electrification process in the system. These values are computed to be about 0.37e with the adsorption of hydrogen and up to 0.24e with the adsorption of carbon monoxide. Training of the system potential energies using the neural network method shows promising opportunity to study further complex problems in such systems.

Key words— Neural networks, machine learning, density functional theory calculations, hydrogen, carbon monoxide, platinum, fuel cells.

1 INTRODUCTION

One of the common applications of Platinum is in a build up of a polymer electrolyte fuel cells (PEMFC). It has proven to be the standard catalyst for many oxidation and reduction reactions in both acidic and basic electrolytes and would be an ideal candidate for high power catalysts. Fuel cells have the potential to be clean and efficient way to run cars, computers, and power stations, where Platinum is an exciting component as catalyst [1]. H_2 and O_2 molecules are among the ions expected to dominate in the electrolyte region of the cells. A study of Interactions of such molecules with the surfaces are catching interests of many works [2], [3].

Author's e-mail: kenate.nemera@gmail.com
Article history: Received March 2019,
Accepted April 2019.

Atomistic calculations are nowadays being actively used to study systems at atomic, molecular, or large length scales. The calculations often involve the obtaining of potential energy surface (PES), where the PES describes the potential energy of a system as a function of the atomic nuclei positions. Atomic interactions within large many body systems often have complicated forms where the exact value is impossible to determine. As a result, only either a crude or reasonable approximations have been enabling a study of problems in such systems, where among those one is a density functional theory method (DFT) [4].

DFT method uses reasonable approximations, and so as such enabled a study of a relatively larger systems which would otherwise be impossible to make in a feasible time. However, the studies of many more properties such as ligand interactions with protein macromolecules, mechanical and electro-mechanical field effects, response of nanostructures to loadings in material science, etc, still require improved computational methodologies or computing speeds than the currently available facilities. This bottleneck in the computational power can be expected to persist in the forseeable future.

While the use of multiscale methods is seen as a solution strategy for a study of problems in such systems, applications of such methodologies is impractical at the present condition of the computing power. Due to a large set of Kohn-Sham density functional theory (KS-DFT) equations required to be solved, it becomes time consuming to solve problems of large systems. As a result, in an attempt of studying problems in many complex systems, multiple alternative simulation methods such as machine

learning of electronic structure methods combined with monte carlo simulations [5], and also machine learning of electronic structure methods combined with molecular dynamics simulations [6], [7], [8], [9], [10], [11] are on the rise. Such approaches would undoubtly be expected to be chosen by many as fronts of research over the next couple of years. In this paper, we emphasize on machine learning using neural network architecture where an electronic structure method is a trainee. Ever since of early works on machine learning [12] and neural network conceptuals [13] for a use in scientific research [14], now there are dozens of papers made available in various journals [6], [7]. We choose the approach of Behler et al [6], for building higher dimensional potential energy surfaces from the electronic structure calculations, and use the implementation in machine learning according to the works by Peterson group at Brown University [15].

Nowadays, the presence of many DFT calculators interfaces in atomic simulation environment (ASE) [16] has made it easy to use atomic models along with DFT codes in a single python script instruction. With recent facility of Amp [17] being also accessible in ASE package, it is possible to make use of interactive collaboration of Amp with electronic structure calculators within ASE.

While such approach would be useful in being applied to solve various real problems in materials over the near futures, here in this work, we apply it to study adsorptions on Platinum surfaces. The current work, thus, has two fold purposes. First, it gives insight on how to develop this approach of study further so to be able to get detail insights into problems in real materials such as fuel cells. Secondly, reactivities of various surfaces of Platinum with molecules: H_2 , O_2 , and CO is studied using the current progress, and the result of this can be seen as a phenomena taking place on some part of real fuel cells. A brief look at the inside outlook of the a proton membrane fuel cell can be seen as in the Fig. 1, where the following basic equations can be seen to take place.

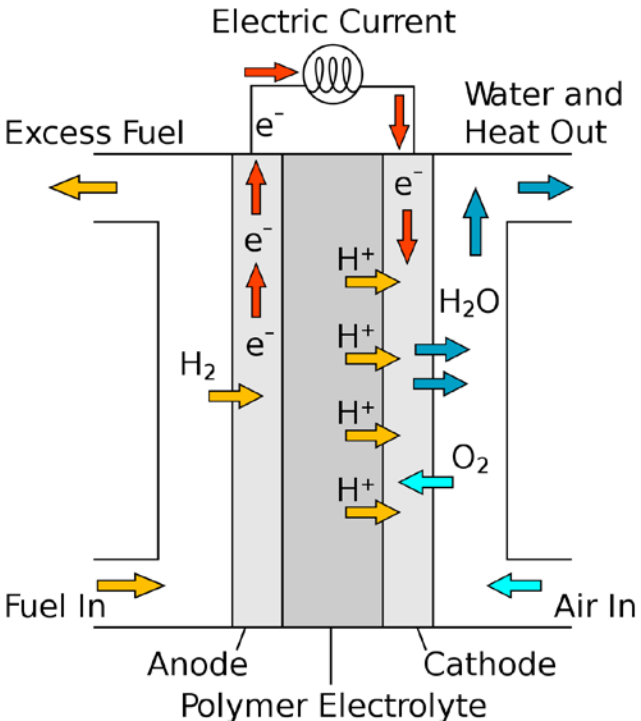

Figure 1: The inside of a polymer electrolyte fuel cells where the anodes and cathodes are made of platinum metals. The dissociative and combination reactions are supposed to take place at anodes and cathodes where platinum acts as a catalyst, see equation equations (1)-(4).

$$CO + Pt \rightarrow Pt - CO \quad (1)$$

$$H_2 + 2Pt \rightarrow 2(Pt - H) \quad (2)$$

$$2(Pt - H) \rightarrow 2H^+ + Q_{ads} + 2Pt \quad (3)$$

$$H_2O + (Pt - CO) \rightarrow P\,t + CO_2 + 2H^+ + Q_{ads}\,, \quad (4)$$

where Q ads is the charge received and then donated by the adsorbate upon interacting with the Platinum surfaces, see Tables in section 3. The paper is organized as follows. In the next section sec. 2, detail account of the computational method is presented. Results and discussions are presented in section 3, with the conclusion presented in section 4.

2 METHODS

We have used two different flavors of numerical simulations: the density functional theory method, and the atomistic machine learning (ML) method, as described below.

2.1 DFT method

The calculations required for this work were performed using an Ab-initio Simulation Package called GPAW [18], [19], [20]. Gpaw has a capacity to compute a total energy, a charge density, and the electronic structure of a periodic systems composed of electrons and nuclei based on pseudopotentials and a plane wave basis. The program is based on density functional theory (DFT) in the Kohn-Sham scheme [4]. All information about the Gpaw package can be found at the homepage [21]. The electron wavefunctions are expanded in a plane wave having

a band, a k-points, and a grid index. The corresponding electron density is given as a sum over the squared wave-function. The k-points grid are produced according to Monkhorst-Pack scheme [22] , in what is some times called as special points, and which results to a set of points equally spaced in the Brillouin zone (BZ) that are not related to each other by any symmetry operation. Periodic boundary conditions are applied to the unit cell, and the plane waves cut off energy used is 400 eV. A k-point mesh of 4×4×1, 2×4×1, and 2×2×1 are used in (1×1), (2×1), and (2×2) surface unit cells, respectively. These results to up to about 16 optimized k_i's within BZ. The exchange-correlations energies are approximated within the the generalized gradient approximation of PBE [23]. The pseudopotentials for the interactions of valence electrons with ion-cores were represented by the plane wave based implementation of the projector augemented wave (paw) method [24], [25]. The number of valence electrons considered in the pseudopotential code is Pd: 10, C: 4, and O: 6. A van der Waals treatment of DFT-D3 type based on the works in literatures [26] is applied, and is found to improve the energetics by up to 0.5 eV. The influence of zero point energy on the energetics of the adsorption is less than 0.1 eV. So, the calculations work presented for our system excluded the effect of the latter conceptual [27].

Adsorption energies are calculated by

$$E_{ads} = -(E_{SM} - E_S - E_M), \quad (5)$$

Here, E_S , E_M , and E_{SM} are the total energies of the clean surface, isolated molecule, and relaxed geometry containing both substrate and molecule, respectively. All energies are per supercell. The isolated molecules are relaxed in a cubic unit cell of side length 15 Å. A vacuum layer of 10 Å is used in all the adsorption calculations. As such, positive values in energies indicate exothermic reactions while negative values denote endothermic. The vibrational frequencies are obtained by diagonalization of the Hessian Matrix which in turn is constructed by finite diference method where every atom is displaced along the three orthogonal directions by 0.015 Å. Complete structural optimitions of the microscopic (atomic coordinates) and macroscopic (unit cell) degrees of freedom are obtained using Hellmann-Feynman forces [28] and stresses [29]. Ab-initio molecular dynamics (MD) is done using the Hellmann-Feynman forces calculated on the Born-Oppenheimer (BO) surface [30] The convergence criteria for the forces were set at 0.1 meV/Å. The bader analysis [31] of charges is based on work by Henkelman et al. [27] and Sanville et al. [32]. The reaction paths are calculated with the nudged elastic band (NEB) method [33], [34], and the minimum energy paths are searched for using a quasi- Newton iterative scheme by mapping out images between two preset geometries.

2.2 Atomistic machine learning method

A neural network based on the concepts suggested by Behler-Parrinello [6] and implemented using atomistic machine learning package (Amp) [17] is used. Such a new approach of using models derived by machine learning (ML) has started during the past decade. In this approach, a large databases of calculations from density functional theory is used to build neural network models of atomistic systems.

A lot of progress has been made in recent years in the development of atomistic potentials using ML techniques. ML potentials rely on simple but very flexible mathematical terms without a direct physical meaning [35]. In case of ML potentials, the topology of the potential energy surface is learned by adjusting a number of parameters with the aim to reproduce a set of reference electronic structure data as accurately as possible. Consequently, in ab-initio molecular dynamics (MD), the energies and forces need to be calculated "on-the-fly", typically using density functional theory (DFT). Alternatively, an analytic expression for the potential energy surfaces (PES) can be constructed and used in the simulations, which allows to perform MD simulations more efficiently as the evaluation of such expressions is much faster than solving the quantum mechanical problem.

Artificial neural networks (NNs) [36], [37] have been introduced in 1943 to model and understand the signal processing in the brain [38], and in the following decades they have found wide use in many fields of science [39] due to their pattern recognition and data classification capabilities. There are many types of NNs with different functional forms. A general definition covering all these types has been given by Kohonen [40]. Artificial neural networks are massively parallel interconnected networks of simple (usually adaptive) elements and their hierarchical organizations which are intended to interact with the

objects of the real world in the same way as biological nervous systems do. For modelling a PES, the input layers are the Cartesian-coordinates of a system with a fixed number of atoms. The nodes of the hidden layers are linear combinations of these coordinates with varying weights. The flexible nature of these models makes them ideal candidates for advanced simulation, such as (monte carlo) MC and MD applications. Standard multilayer feed-forward networks with as few as one hidden layer using arbitrary squashing functions are capable of approximating any function from one finite dimensional space to another to any desired degree of accuracy, provided that sufficiently many hidden units are available.

Within this way of constructing the atomistic potentials, the remarkable resultis that there is no fundamental restriction in the accuracy that can be achieved when constructing potentials using neural networks (NNPs), which is an important difference to physical potentials having intrinsic limitations due to their rather inflexible functional forms. In the past two decades, NNPs have been constructed for many types of systems.

Most conventional NNPs use a single machine learning feed-forward neural network (MLFF NN) to construct a direct functional relation between the atomic configuration and the potential energy. For this purpose, a number of artificial neurons is organized in several layers. The potential energy E is obtained in the neuron, or node, in the output layer. A typical NN architecture contains two to three hidden layers and up to typically about 50 nodes per layer. The entity of all layers including the input and output layer as well as the number of nodes per layer defines the architecture of the NN.

The total energy of the system is given as

$$E_s = \sum_{i=1}^{N_{\text{atom}}} E_i \quad (6)$$

where, E_s − is energy of the system, and E_i − is atomic energy contributions. The atomic energy contributions depend on the local chemical environments up to a cutoff radius R_c . This cutoff radius, which typically has a value between 6 and 10 Å, is a convergence parameter and needs to be tested to ensure that all energetically relevant interactions are included. The positions of the neighboring atoms within the resulting cut-off sphere are then described by a set of many body symmetry functions. The resulting high dimensional NN approach composes the following. For each atom, there is a separate line starting from the Cartesian coordinate vector R of the atom. In the next step, a vector of many body symmetry functions G is constructed for each atom, which describes the arrangement of all atoms in the chemical environment.

By defining a cutoff radius large enough for all atomic interactions to be taken into consideration, the system needs only calculate and sum the energy contribution of each local environment to obtain the total energy. For example, a system of two gas-phase atoms in the ideal gas limit can be described by the six Cartesian-coordinates of the atoms, but in this simple case the single variable which represents the distance between the two atoms is sufficient to represent the entire PES. This way, only one feed-forward NN per type of element is needed. This approach makes a very diverse range of applications accessible to a single potential. It also creates an opportunity for combining a more diverse range of training sets which creates future possibilities for more chemically advanced applications. We have studied how DFT should be trained to get a Behler-Parrinello neural network (BPNN) atomistic potentials which is accurate and tractable across multiple structural regimes of palladium material.

The Behler-Parrinello NN produced with the lowest root-mean-squared error (RMSE) was used in this work. This NN utilises 2 hidden layers with 2 and 12 nodes and a hyperbolic tangent activation function. A total of 20 symmetry functions were used for all atoms of adsorbate, and Pd for a total of 40 functions.

Studies of some insight into reaction processes within the fuel cell systems are modelled with adsorptive interactions, where the adsorbate are attached to the surfaces with single, bi-, and tri-, coordination numbers with the surfaces, denoted respectively, as hollow (H), bridge (B), and atop (T), respectively, as shown in Fig. 2.

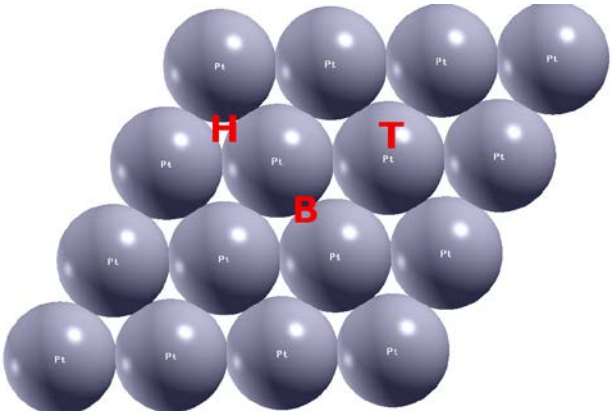

Figure 2: Top view of surface Pt atoms. Color online: Colors (dark grey- Pt atoms). Adsorption sites are indicated by red color bold face letters, where H-means hollow site, B-means bridge site, and T-means atop sites. These terms are to be used frequently in the presentation of the results in section 3.

3 RESULTS AND DISCUSSIONS

The calculated lattice constant and Bulk modulus of the Face centered cubic structure of the Platinum system is a =3.97 Å and B = 268.05 GPa, respectively. These values are closely related to experimental works a =3.96 Å [41], a =3.96 Å [42] and theoretical works of a =3.91 Å [42]. The author believes that these closely related outcomes validate the methods (section 2.1) used in this study. Stabilities of surfaces prior to the adsorptive interaction can be determined according to the equation

$$\sigma = \frac{1}{2}\left(E_{\text{slab}} - \frac{N_{\text{slab}}}{N_{\text{bulk}}} E_{\text{bulk}}\right)$$

where, E_{slab} refers to total energy of symmetric slab, N_{slab} refers to number of atoms in the slab, N_{bulk} refers to number of atoms in the bulk unit cell, and E_{bulk} is total energy of a bulk unit cell. Accordingly, the surface energy and hence the stability of Pt(111) > Pt(100) > Pt(110) > Pt(211). Such studies of surface energies is often calculated [43] and the implications are there described. Within the study of the adsorptive interaction of these surfaces with adsorbate molecules carbon monoxide and hydrogen, the outcomes of the investigation is presented in the the following subsections.

3.1 Pt(100) surface

With the adsorption of carbon monoxide on Pt(100) surface, Table 1, adsorption energy increases according to $E_{\text{ads}}^{B} > E_{\text{ads}}^{T} > E_{\text{ads}}^{H}$, where B-, T -, and H-, denote bridge, top, and hollow adsorption sites, respectively, see Fig. 2. The vibration energy can be related to the vibration frequency according to $E_{vib} = hcv$. With this, the vibration energies are 0.23 eV, 0.20 eV, and 0.19 eV, respectively, at atop, bridge, and hollow sites. Accordingly, all the vibration energies are within measures of error [44] and do not exceed 0.20 eV.

Table 1: Adsorption of CO and H_2 molecules on Pt(100) surface, as calculated using DFT method (section 2.1). Adsorbate coverage is given in mono-layer (ML) where 1 ML means 1 adsorbate species per surface slab supercell. Thus, 1 ML means adsorption on (1×1) surface unit cells. E_{ads} means adsorption energy in eV, v means vibration frequency of the bond between surface Pt atoms and adsorbate in unit cm^{-1}, ΔQ_{pt} represents change in magnitude of charge of surface Pt atom in unit *e*, and ΔQ_{ads} represents change in magnitude of charge of adsorbate atom in unit *e*.

CO					
CO coverage [ML]	Adsorption site	E_{ads} [eV]	v [cm^{-1}]	ΔQ_{pt} [e]	ΔQ_{ads} [e]
1	atop	1.38	1984.89	-0.11	+0.11
	bridge	1.80	1814.69	-0.17	+0.17
	hollow	0.85	1745.79	-0.37	+0.37
H_2					

H_2 coverage [ML]	Adsorption site	E_{ads} [eV]	v [cm^{-1}]	ΔQ_{pt} [e]	ΔQ_{ads} [e]
1	atop	1.49	2448.16	-0.02	+0.02
	bridge	1.88	984.09	-0.05	+0.05
	hollow	1.61	133.62	-0.02	+0.02

This means that such considerations can be overlooked since the impacts on the total adsorption energy is negligible. However, the trends in the vibration energies tell us something about the strength of the bonding between the adsorbate and the surface atoms. Accordingly, it appears that in terms of the stability of the bounding of the adsorbate, adsorption at H > B > T . From charge transfer point of view, relatively a larger charge transfer takes place at hollow site followed by at bridge site, and at atop sites. While this ordering is similar to that with vibration, it is slightly different from that with the adsorption energies. While vibrations and charge transfers relate to coordination numbers, adsorption energies seem to greatly depend on lateral interactions. That is, at this adsorbate coverage, lateral interactions between adsorbates is weaker for adsorption at hollow site followed by adsorption at atop site followed by adsorption at bridge site. Regarding adsorption of H_2 on the Pt(100) surface, the adsorption energy increases according to:

$E_{\text{ads}}^{B} > E_{\text{ads}}^{H} > E_{\text{ads}}^{T}$. With the vibration energies calculable with as described above, the values are 0.28 eV, 0.11 eV, and 0.01 eV, respectively, for atop, bridge, and hollow sites. Correspondingly, thus, the stability of the adsorbate with the surfaces appears to increase according to hollow followed by at bridge site followed by at atop site. With charge, large charge transfer is for adsorption at bridge site followed by with about equals of the adsorptions at hollow and atop sites. In this case, while analysis with charge transfers and adsorption energies indicate similar trends regarding the strengths of the adsorptions, analysis with vibrations indicate slightly a different trend. However, in summary, adsorption at bridge site seems to be the most preferred at 1 ML of the adsorbate coverage on the Pt(100) surface.

3.2 Pt(111) surface

Here adsorption of CO and H_2 molecules from 0.25 ML - 1 ML is studied, Table 2. With the adsorption of CO molecule, the adsorption energies in ascending order is seen as: $E_{\text{ads}}^{B} > E_{\text{ads}}^{H} > E_{\text{ads}}^{T}$ at 1 ML.

At 0.5 ML, $E_{\text{ads}}^{H} > E_{\text{ads}}^{B} > E_{\text{ads}}^{T}$ and at 0.25 ML,$E_{\text{ads}}^{B} > E_{\text{ads}}^{H} > E_{\text{ads}}^{T}$.

Table 2: Adsorption of CO and H_2 molecules on Pt(111) surface, as calculated using DFT method (section 2.1). Adsorbate coverage is given in mono-layer (ML) where 1 ML means 1 adsorbate species per surface slab supercell. Thus, 1 ML means adsorption on (1×1), 0.5 ML means adsorption on (2×1), and 0.25 ML means adsorption on (2×2) surface unit cells. E_{ads} means adsorption energy in eV .

CO			H_2		
CO coverage [ML]	Adsorption site	E_{ads} [eV]	H_2 coverage [ML]	Adsorption site	E_{ads} [eV]
1	atop	0.89	1	atop	1.30
	bridge	0.92		bridge	1.76
	hollow	0.91		hollow	1.63
0.5	atop	1.35	0.5	atop	1.52
	bridge	1.81		bridge	1.63
	hollow	1.82		hollow	1.82
0.25	atop	1.25	0.25	atop	1.56
	bridge	1.92		bridge	1.71
	hollow	1.38		hollow	1.23

So, it appears, more of, that adsorption at bridge site is more energetic in the coverage range of [0.5,1.5] ML, while adsorption at hollow site is expected to be

more energetic in the coverage range [0.25,1.0] ML, and while adsorption at top site is expected to be more energetic at the coverage range of above 2 ML.

With the adsorption of H_2 , a similar pattern of adsorption as with that of CO is observed as can be seen from Table 2. Pronouncedly, however, the adsorption energetics of H_2 is slightly larger than that of CO at 1 ML. These values are comparable to literatures [45], [46], while the calculations are being subjected to errors of about 0.2 eV [44]. In addition, the results in this work would also answer some of the concerns raised in the literatures [47], [46].

3.3 Pt(211) surface

At 1 ML, $E_{\text{ads}}^{B} > E_{\text{ads}}^{H} > E_{\text{ads}}^{T}$. Charge transfer between adsorbate CO and the surface Pt atoms is as much as 0.18e, see Table 3, while for between H_2 and the surface Pt atoms, as much as of 0.24e charge transfer can take place. The adsorption energetics of CO is slightly larger than that of the adsorption energetics of H_2 . The adsorption energies at 1 ML for CO, the adsorption energies increase according to: adsorption on Pt(211) followed by adsorption on Pt(100) followed by adsorption on Pt(111) surface. Adsorption of H_2 however has about the same energetics in all the surfaces. The biggest charge transfer on this surface is with CO, which is of about 0.37e. Our values of the adsorption energies of hydrogen is higher than those in literatures [2] but is in a good agreement elsewhere [45], [2].

With calculation using neural network approach of section 2.2, adsorption energies are estimated with variations and identicalness as shown in Figures 3 and 4. With the adsorption of CO (Figure 3), on the Pt(110) surface, the adsorption energies are predicted to be about the same using both with the neural network approach of section 2.2 and the DFT method of section 2.1.The energy differences are less than 0.01 eV for all the adsorption sites on this surface. The energy differences are investigated to be largest for adsorption at the ontop site, which is about 0.9 eV, and this happens on the Pt(100) surface. According to the energy differences, $\Delta E = E_{\text{ads}}^{\text{NN}} - E_{\text{ads}}^{\text{DFT}}$, between the calculations using neural network and DFT methods, the variations in the energies are according to: on Pt(100) > Pt(111) > Pt(211) > Pt(110).

Table 3: Adsorption of CO and H_2 molecules on Pt (211) surface, as calculated using DFT method (section 2.1). Adsorbate coverage is given in mono-layer (ML) where 1 ML means 1 adsorbate species per surface slab supercell. Thus, 1 ML means adsorption on (1×1) surface unit cells. E_{ads} means adsorption energy in eV , ΔQ_{pt} represents change in magnitude of charge of surface Pt atom in unit e, and ΔQ_{ads} represents change in magnitude of charge of adsorbate atom in unit e.

CO				
CO coverage [ML]	Adsorption site	E_{ads} [eV]	ΔQ_{pt} [e]	ΔQ_{ads} [e]
1	atop	1.78	-0.11	+0.11
	bridge	2.08	-0.18	+0.18
	hollow	2.08	-0.17	+0.17
H_2				
H_2 coverage [ML]	Adsorption site	E_{ads} [eV]	ΔQ_{pt} [e]	ΔQ_{ads} [e]
1	atop	1.43	-0.01	+0.01
	bridge	1.89	-0.06	+0.06
	hollow	1.60	-0.24	+0.24

This means, more concerted effort on training of the ab-initio calculations is recommended for Pt(100), Pt(111), and Pt(211).

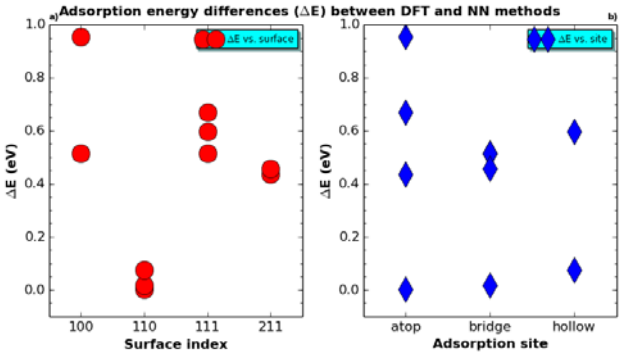

Figure 3: Energy differences (ΔE) between adsorption energies of CO as calculated using the DFT (section 2.1) and the neural network (section 2.2) methods. Adsorption energies are calculated for the lower indices of the Platinum surface, i.e., Pt(100), Pt(110), Pt(111), and Pt(211) surfaces, denoted respectively as (100), (110), (111), and (211) in the figures. On the left side (a) (red color and filled circle points), energy differences are plotted against surfaces while on the right side (b) (blue color and thin diamond points) , energy differences are plotted against adsorption sites.

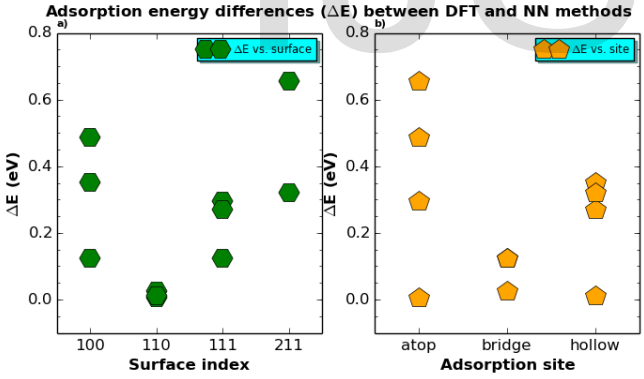

Figure 4: Energy differences (ΔE) between adsorption energies of H_2 as calculated using the DFT (section 2.1) and the neural network (section 2.2) methods. Adsorption energies are calculated for the lower indices of the Platinum surface, i.e., Pt(100), Pt(110), Pt(111), and Pt(211) surfaces, denoted respectively as (100), (110), (111), and (211) in the figures. On the left side (a) (green color and thick hexagonal points), energy differences are plotted against surfaces while on the right side (b) (orange color and pentagonal points), energy differences are plotted against adsorption sites.

With the adsorption of H_2 , the least variation in ΔE is investigated on Pt(110) which means that the potential is well trained on this surface. ΔE has as much as 0.7 eV on Pt(211) surface, while it is as much as of 0.50 eV on Pt(100), and 0.35 eV on Pt(111) surfaces. This means for surfaces which show large variation in the energy differences (ΔE), more training is needed. The influences of these on the adsorption sites is more pronounced with the atop site which has ΔE of about 0.65 eV followed by at hollow site by up to 0.40 eV, which in turn is followed by bridge site with about 0.15 eV. While the trends of ΔE in Fig. 4 is similar with the trends in Fig. 3, the magnitudes of the energy differences in the former case is relatively smaller due to in part the smaller number of electrons contained in the H_2 adsorbate when as compared to the CO adsorbate and which would in turn thus require more training efforts to get it right. Analysis and comparison of the charge transfers with the adsorption of the adsorbate molecules can be visualized as in the Fig.5. To achieve a well trained potential, more training efforts are often required to be done [35], [7]. Studies of the interactions of these molecules can be useful to remedy the efficiencies of performances this system as an application in fuel cells [48], [49].

4 CONCLUSION

The outcomes of this study of adsorptions on platinum surfaces is summarized as follows.

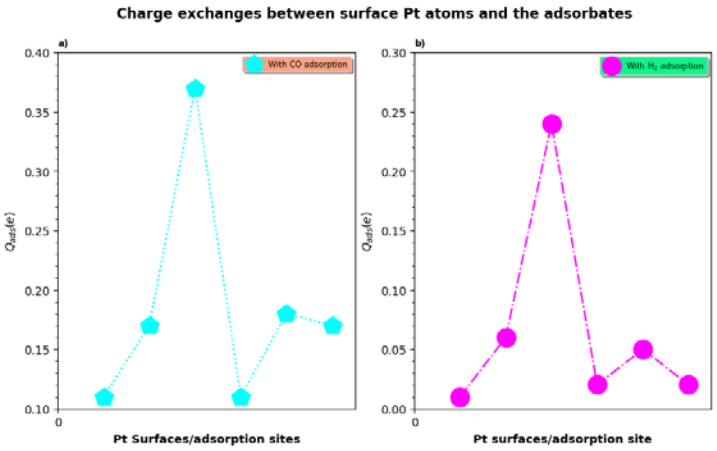

Figure 5: Charges exchanges between surface atoms and adsorbates. a) Left side (pentagonal points and cyan color for the adsorption of CO on Pt surface). b) Right side (Filled circle points and magenta color for adsorption of H_2 on Pt surface).

- Adsorption energies in the range of [0.85, 2.08] eV is investigated for adsorption of CO, while the adsorption energies in the range of [1.30, 1.90] eV is investigated for adsorption of hydrogen.
- Charge transfers of upto 0.37e is investigated with adsorption of hydrogen while that of upto 0.24e is investigated with adsorption of CO.
- The molecules hydrogen and carbon monoxide react strongly with platinum surfaces. Such strong interactions in terms of adsorption energies and charges could mean facilitated electricity as of Figure 1 and a more likely formation of by-products as of equations (1)-(4).
- There is a strong possibility that training the DFT potentials could very well be used in related problems thereby reducing the computing time demand in many future problems solving.
- Since problems study in fuel cells require a more dynamic transport phenomena modelling than studying from statical point of view, such neural network method would have a favourable prospect to be a feasible method of dealing with problems in such systems.
- Most stable surfaces are relatively less reactive means stepped surfaces provide more opportunities for reactions.
- While still many more training efforts needed can be done, the current work explores many prospects of further studies quantitative and qualitative wise.

Acknowledgments

This work has started at Carnegie Mellon University at PA, USA, and then remarkably refined using a different software packages at the present address of the author. The US Department of State is greatly appreciated for the financial support during visitor's stay at the abroad University.

Disclosure statement

The author declares that there is no conflict of interest.

References

[1] R. Sekol, X. Li, P. Cohen, G. Doubek, M. Carmo , A. Taylor, Silver palladium core-shell electrocatalyst supported on mwnts for orr in alkaline media, Applied Catalysis B: Environmental 138-139 (2013) 285.

[2] Y. Yu, J. Yang, C. Hao, X. Zhao, Z. Wang, The adsorption, vibration and diffusion of hydrogen atoms on platinum low-index surfaces, Journal of Computational and Theoretical Nanoscience 6 (2009) 439.

[3] P. Ferrin, S. Kandoi, A. Nilekar, M. Mavrikakisy, Atomic and molecular adsorption on Pd(111), Surf. Sci. 606 (2012) 679.

[4] W. Kohn, L.J. Sham, Self-consistent equations including exchange and correlation effects, Phys. Rev. 140 (1965) A1133.

[5] F. Geng, J. Boes, J. Kitchin, First-principles study of the Cu-Pd phase diagram, Calphad 56 (2017) 224.

[6] J. Behler, M. Parrinello, Generalized Neural Network Representation of High Dimensional Potential Energy Surfaces, Phys. Rev. Lett. 98 (2007) 146401.

[7] J. Boes, J. Kitchin, Neural network predictions of oxygen interactions on a dynamic pd surface, Molecular Simulation 43 (5-6) (2017) 346.

[8] N. Artrith, T. Morawietz, J. Behler, High dimensional neural network potentials for multicomponent systems: Applications to zinc oxide, Phys. Rev. B 83 (2011) 153101.

[9] J. Behler, Atom-centered symmetry functions for constructing high dimensional neural networks potentials, J. Chem. Phys. 134 (7) (2011) 074106.

[10] E. Belisle, Z. Huang, S. Digabel, A. Gheribi, Evaluation of machine learning interpolation techniques for prediction of physical properties, Comput. Mat. Sci. 98 (2015) 170.

[11] N. Artrith, A. Urban, An implementation of artificial neural network potentials for atomistic materials simulations: Performance for TiO_2 , Comput. Mat. Sci. 114 (2016) 135.

[12] F. Rosenblatt, The perceptron: A probabilistic model for information storage and organization in the brain, Psychol. Rev. 65 (1958) 386.

[13] W. McCulloch, W. Pitts, A logical calculus of the ideas immanent in nervous activity, Bull. Math. Biophys. 5 (1943) 115.

[14] Y. Hu (Ed.), Handbook of Neural Network signal processing, CRC press, inc., Boca Raton, USA, 2000.

[15] Amp documentation lives at https://amp.readthedoc.io.

[16] ASE package is available at https://wiki.fysikdtu.dk.

[17] A. Khorshidi, A. Peterson, Amp: A modular approach to machine learning in atomistic simulations, Comput. Phys. Commun. 207 (2016) 310.

[18] J. J. Mortensen, L.B. Hansen, and K. W. Jacobsen, Real-space grid implementation of the projector augmented wave method, Phys. Rev. B 71(3) (2005) 35109.

[19] J. Enkovaara, C. Rostgaard, J. J. Mortensen et al, Electronic structure calculations with GPAW: a real-space implementation of the projector augmented-wave method, J. Phys.: Condens. Matter 22 (2) (2010) 253202.

[20] J. Enkovaara, N.A. Romero, S. Shende, J.J. Mortensen, GPAW - massively parallel electronic structure calculations with Python-based software, Procedia Computer Science 4 (2011) 17-25.

[21] https://wiki.fysik.dtu.dk/gpaw (last updated: March 2019).

[22] H. Monkhorst, J. Pack, Special points for brillouin-zone integrations, Phys. Rev. B 13 (1976) 5188.

[23] J. Perdew, K. Burke, M. Ernzerhof, Generalized gradient approximation made simple, Phys. Rev. Lett. 77 (1996) 3865.

[24] P. Blochl, Projector augmented-wave method, Phys. Rev. B 50 (1994) 17953.

[25] P. E. Blöchl, C. J. Först, J. Schimpl, Projector augmented wave method: ab-initio molecular dynamics with full wave functions, Bull. Mater. Sci. 26 (1) (2003) 33-41.

[26] J. Moellmann, S. Grimme, Dft-d3 study of some molecular crystals, J. Phys. Chem. C 118 (14) (2014) 7615.

[27] G. Henkelman, A. Arnaldsson, H. Jonsson, A fast and robust algorithm for bader decomposition of charge density, Comput. Mater. Sci. 36 (2006) 354.

[28] P. Feynman, Forces in molecules, Phys. Rev. 56 (1939) 340.

[29] O. Nielsen, R. Martin, Quantum mechanical theory of stress and force, Phys. Rev. B. 32 (1985) 3780.

[30] R. Wentzcovitch, J. Martins, First principles molecular dynamics of Li: Test of a new algorithm, Solid State Commun. 78 (1991) 831.

[31] R. Bader, Atoms in Molecules. A Quantum Theory, Oxford University press, Clarendon, 1990.

[32] E. Sanville, S. D. Kenny, R. Smith, G. Henkelman, Improved grid-based algorithm for bader charge allocation, J. Comp. Chem. 28 (2007) 899.

[33] H. Jonsson, G. Mills, K. W. Jacobsen, Classical and Quantum Dynamics in Condensed Phase Simulations, World Scientific, Singapore, 1998.

[34] G. Henkelman, H. Jonsson, Improved tangent estimate in the nudged elastic band method for finding minimum energy paths and saddle points, J. Chem. Phys. 113 (2000) 9978.

[35] J. Behler, Constructing high dimensional neural network potentials: A tutorial review, International Journal of Quantum Chemistry 115 (2015) 1032.

[36] C. M. Bishop, Neural Networks for Pattern Recognition, Oxford University press, Oxford, 1996.

[37] S. Haykin, Neural Networks and Learning Machines, Prentice Hall, New York, 2009.

[38] W. McCulloch, W. Pitts, A logical calculus of the ideas immanent in nervous activity, Bull. Math. Biophys. 5 (1943) 115.

[39] J. Gasteiger, J. Zupan, Neural networks in chemistry, Angew. Chem. Int. Ed. 32 (1993) 503.

[40] T. Kohonen, An introduction to neural computing, Neural Networks 1 (1988) 3.

[41] P. Haas, F. Tran, P. Blaha, Calculation of the lattice constant of solids with semilocal functionals, Phys. Rev. B 79 (2009) 085104.

[42] W. P. Davey, Precision Measurements of the Lattice Constants of Twelve Common Metals, Phys. Rev. 25 (1925) 753.

[43] L. Vitos, A. Ruban, H. Skriver, J. Koller, The surface energy of metals, Surf. Sci. 411 (1998) 186.

[44] ”Adsorption energies as calculated using different assumptions in DFT codes can result to differences in energies by as much as of 0.2 eV.”

[45] C. Ma, T. Liu, L. Chen, A computational study of H_2 dissociation and CO adsorption on the Pt_{ML}/WC(0001) surface, Applied Surface Science 256 (2010) 7400–7405.

[46] P. Philipsen, E. Lenthe, J. Snijders, E. Baerends, Relativistic calculations on the adsorption of CO on the (111) surfaces of Ni, Pd, and Pt within the zeroth-order regular approximation, Phys. Rev. B 56 (1997) 13556.

[47] P. J. Feibelman, B. Hammer, J. K. Norskov, F. Wagner, M. Scheffler, R. Stumpf, R. Watwe, J. Dumesic, The CO/Pt (111) puzzle, J. Phys. Chem. B 105 (2001) 4018.

[48] J. Baschuk, X. Li, Carbon monoxide poisoning of proton exchange membrane fuel cells, Int. J. Energy Res. 25 (2001) 695.

[49] S. Ehteshami, Q. Jia, A. Halder, S. Chen, S. Mukarjee, The role of electronic properties of Pt and Pt alloys for enhanced reformate electro-oxidation in polymer electrolyte membrane fuel cells, Electrochimica Acta 107 (2013) 155.